Nanoscale Horizons

ROYAL SOCIETY OF CHEMISTRY

COMMUNICATION

View Article Online
View Journal | View Issue

Cite this: *Nanoscale Horiz.*, 2026, **11**, 225

Received 15th July 2025,
Accepted 14th October 2025

DOI: 10.1039/d5nh00492f

rsc.li/nanoscale-horizons

Supramolecular DNA/amino acid-based oxidase-mimetic nanocatalysts exhibiting drug degradation capability

Mengjie Yu,† Xianxue Zhang,† Shichao Xu and Zhen-Gang Wang *

Developing efficient and environmentally benign approaches for the remediation of antibiotic pollutants has become a paramount research imperative, since the extensive use of antibiotics has raised serious concerns due to their potential to induce antibiotic resistance and disrupt the ecological balance. In this work, we report the self-assembly of fluorenylmethyloxycarbonyl-lysine (Fmoc-K) aggregates with natural calf thymus DNA (CT-DNA) and Cu^{2+} to construct a catalyst that possesses copper-dependent active sites, mirroring the catalytic function of laccase, an oxidase known for its ability to degrade phenolic antibiotics. Structural characterization, including circular dichroism, fluorescence spectroscopy, transmission electron microscopy (TEM) and electron paramagnetic resonance (EPR), indicates the association of Fmoc-K with DNA components, facilitating the coordination of Cu^{2+} to both. Kinetic studies revealed that the Fmoc-K/CT-DNA/Cu^{2+} complex exhibited over 13-fold higher catalytic efficiency than either CT-DNA/Cu^{2+} or Fmoc-K/Cu^{2+} alone. Notably, CT-DNA not only serves as a structural scaffold but also promotes the access of antibiotic substrates (including doxorubicin and tetracycline) to the copper center due to its binding affinity for these antibiotics, thereby facilitating efficient oxidative degradation. This work offers a promising strategy for constructing high-performance, environmentally responsive metalloenzyme mimics for pollutant remediation.

New concepts

We report a supramolecular oxidase-mimetic nanocatalyst assembled from fluorenylmethyloxycarbonyl-lysine (Fmoc-K), calf thymus DNA (CT-DNA), and Cu^{2+} ions. This catalyst mimics laccase-like activity with significantly enhanced stability and catalytic performance. The key innovation lies in integrating DNA not only as a structural scaffold but also as a molecular host that binds antibiotics such as doxorubicin and tetracycline, thereby facilitating their proximity to the catalytic copper centers for efficient oxidative degradation. Unlike traditional nanozymes, this system forms coordinatively unsaturated Cu^{2+} sites through Fmoc-driven ordered assembly, enabling over 13-fold higher catalytic efficiency than binary systems. DNA's groove-binding with Fmoc-K helps maintain an open copper coordination sphere, which is often lost in conventional self-assembly. The catalyst also exhibits superior thermal and long-term storage stability compared to natural laccase. This work advances nanoscience by demonstrating how supramolecular interactions and biomolecular recognition can be combined to create functional metalloenzyme mimics. It introduces a new strategy for environmental remediation using biohybrid catalysts, highlighting the untapped catalytic potential of nucleic acid–peptide–metal assemblies.

Introduction

The widespread use of antibiotics in medicine and agriculture has led to their significant accumulation in aquatic environments, raising serious concerns due to their potential to induce antibiotic resistance and disrupt the ecological balance.[1,2] The design of robust, efficient, and environmentally benign strategies for the removal of antibiotic pollutants from aquatic systems has emerged as a critical focus in environmental research. Laccases, a family of multi-copper oxidases (MCOs), catalyze the single-electron oxidative degradation of a broad array of organic substrates, including aromatic and phenolic substances, concomitant with the four-electron reduction of molecular oxygen to water.[3–5] Owing to their catalytic versatility and eco-friendly redox chemistry, laccases have attracted considerable attention as green catalysts for applications in wastewater treatment and soil remediation.[6,7] Like other enzymes, the susceptibility of laccases to environmental changes, the difficulty in structural modification, and the laborious separation and purification severely hamper the large-scale applications of laccases. On the other hand, the structure and activity relationship of enzymes has inspired the development of supramolecular catalysts that leverage the noncovalent interactions to assemble catalytic components to create enzyme-like

State Key Laboratory of Organic–Inorganic Composites, Key Lab of Biomedical Materials of Natural Macromolecules (Beijing University of Chemical Technology, Ministry of Education), Beijing Laboratory of Biomedical Materials, Beijing University of Chemical Technology, Beijing 100029, China.
E-mail: wangzg@buct.edu.cn
† These authors contributed equally to this work.

active sites within synthetic materials, enabling reactions that closely mimic those catalysed by natural enzymes.[8–10] However, their catalytic efficiencies rarely match those of natural enzymes, largely due to the challenges in arranging essential functional groups and constructing well-defined enzyme-like active sites. In particular, *de novo* creation of biomimetic metallocluster active sites (*e.g.* the multicopper centers of laccases) requires precise geometric organization of ligand groups.

Considerable efforts have been made to develop laccase-mimicking catalysts, by employing various molecular building blocks.[11–14] While the formation of multicopper sites through the assembly of ligand-bearing building blocks is relatively straightforward, since adjacent copper ions can be bridged by hydroxide ions in aqueous environments to form di- or tri-copper clusters, the critical challenge lies in preserving the coordinative unsaturation of the copper centers. Flexible ligands in the self-assembly system tend to fully coordinate with copper ions in an effort to lower the chemical potential of the system, often leading to saturated copper sites that are ineffective for O_2 activation. This challenge led to significantly lower catalytic efficiency of the Cu-dependent catalysts than that of native laccase. Our group previously reported the self-assembly of fluorenylmethyloxycarbonyl (Fmoc)-modified amino acids, in which directional stacking of the fluorenyl groups drives the ordered arrangement of ligand groups from the amino acid side chains or backbones, leading to the formation of coordinatively unsaturated dinuclear copper centers.[15] It was also reported that the reactivity of the metal center can be enhanced by utilizing heteroatoms as ligands (*e.g.* N, P).[16–18] In this work, we introduced natural DNA (calf thymus DNA, abbreviated as CT-DNA) to self-assemble with Fmoc-lysine (Fmoc-K) and Cu^{2+} to form a robust laccase-mimicking catalyst (Fig. 1). It was observed that Fmoc-Lys can interact with CT-DNA through groove binding, promoting the coordination of Cu^{2+} to both components, enabling this catalyst to exhibit synergistic oxidative activity. Moreover, CT-DNA has shown great affinity to a variety of antibiotics, such as broad-spectrum cancer-killing doxorubicin and tetracycline. Through CT-DNA/Fmoc-Lys self-assembly, these antibiotics can be brought nearby the copper center, facilitating the efficient degradation of the antibiotics. This work provides a novel paradigm for the design of high-performance metalloenzyme mimics to address emerging antibiotic contaminants under ambient and environmentally relevant conditions.

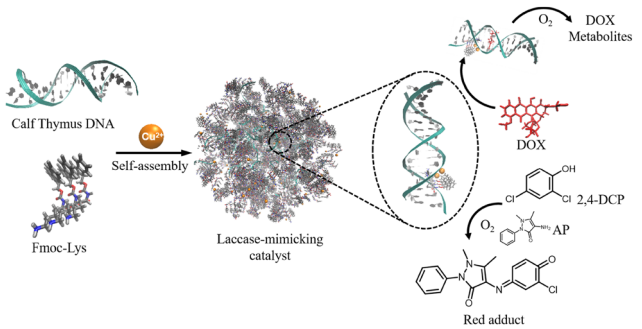

Fig. 1 Self-assembly of calf thymus DNA with Fmoc-Lys and Cu^{2+} to produce copper-dependent oxidase-mimetic supramolecular catalysts for antibiotic oxidative degradation.

Results and discussion

We first utilized the native calf thymus DNA (CT-DNA) to assemble with Cu^{2+} and the amphiphilic Fmoc-lysine (Fmoc-K). TEM imaging showed that Fmoc-K/Cu^{2+} formed nanoscale fibers, which became more aggregated upon the addition of CT-DNA (Fig. 2A and Fig. S2). As a control, CT-DNA/Cu^{2+} existed as particles approximately 1 μm in size (Fig. S1). Fmoc-K exhibited a maximum fluorescence emission at approximately 380 nm (Fig. S3), which is characteristic of a parallel arrangement of fluorenyl rings.[19–22] Notably, the addition of CT-DNA and Cu^{2+} did not significantly alter the fluorescence signal of Fmoc-K, suggesting that the stacking structures of Fmoc-K remained intact (Fig. S3). We employed fluorescence titration to determine the binding affinity. The binding constant (K_A) of Fmoc-K with CT-DNA was estimated as $2.28 \times 10^4\ M^{-1}$ using the Scatchard equation (see details in the Experimental section) (Fig. S6).

Circular dichroism (CD) analysis was performed to further investigate the self-assembly of CT-DNA with Fmoc-K. The CD spectrum of CT-DNA showed a negative band at ~245 nm and

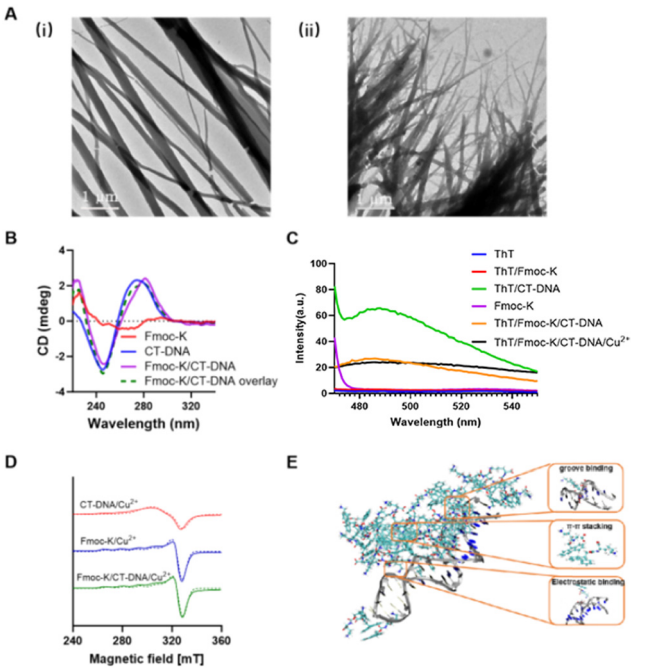

Fig. 2 (A) TEM images of (i) Fmoc-K/Cu^{2+} and (ii) Fmoc-K/CT-DNA/Cu^{2+}. [Fmoc-K] = 1 mM, [CT-DNA] = 91.2 μM bp, [Cu^{2+}] = 5 μM. (B) CD spectra of Fmoc-K, CT-DNA, and the Fmoc-K/CT-DNA complex, along with the spectral overlay of Fmoc-K with CT-DNA. The optical path is 0.5 mm, [Fmoc-K] = 2 mM, and [CT-DNA] = 365 μM bp. (C) Fluorescence spectra of Fmoc-K/CT-DNA/ThT. The excitation wavelength is 450 nm. [Fmoc-K] = 1 mM, [CT-DNA] = 15.2 μM bp, [ThT] = 10 μM, and [Cu^{2+}] = 5 μM. (D) Continuous-wave electron paramagnetic resonance (cw-EPR) of the CT-DNA/Cu^{2+}, Fmoc-K/Cu^{2+} and Fmoc-K/CT-DNA/Cu^{2+} complex. (E) Various interactions present in the theoretical model of Fmoc-K/CT-DNA aggregates.

a positive band at ~275 nm, corresponding to the right-handedness of the classical B-DNA double helix. Fmoc-K exhibited a CD response between 240 nm and 280 nm, which can be attributed to fluorenyl–fluorenyl interactions. Notably, upon the addition of Fmoc-K to CT-DNA, the CD spectrum of Fmoc-K/CT-DNA did not overlap with the superimposed spectra of Fmoc-K and CT-DNA alone, indicating an interaction between Fmoc-K and CT-DNA (Fig. 2B). We also incubated thioflavin T (ThT) with CT-DNA/Fmoc-K hybrids to further identify their binding. When ThT binds to dsDNA, its molecular planarity increases, leading to a significant enhancement of fluorescence intensity, as shown in Fig. 2C. Interestingly, the fluorescence intensity of the CT-DNA/ThT hybrid decreased significantly upon assembly with Fmoc-K, while the Fmoc-K/ThT hybrid exhibited negligible fluorescence. The fluorescence intensity of ThT remained largely unchanged after the addition of copper ions (Fig. 2C). This observation indicates that Fmoc-K and ThT likely both interacted with CT-DNA through groove binding.[23,24] We performed molecular dynamics (MD) simulations to understand the interactions of Fmoc-K with CT-DNA at the molecular level. The CT-DNA model was constructed based on CT-DNA with a GC base content of approximately 42%. During the process of MD, Fmoc-K molecules were observed to aggregate around CT-DNA over time, ultimately forming stable assemblies (Fig. S4 and S5). Multiple interaction modes were identified in the Fmoc-K/CT-DNA assemblies, including groove binding and electrostatic binding between Fmoc-K and CT-DNA, as well as π–π stacking interactions between Fmoc-K molecules (Fig. 2E). We then evaluated the coordination environment of Cu^{2+} by low-temperature X-band continuous-wave electron paramagnetic resonance (cw-EPR) (Fig. 2D). Fmoc-K/Cu^{2+} (g_x, ~2.07, g_y, ~2.07, g_z, ~2.36, and $A_{\parallel}$, ~133 × 10^{-4} cm^{-1}), CT-DNA/Cu^{2+} (g_x, ~2.14, g_y, ~2.14, g_z, ~2.14, and $A_{\parallel}$, ~26.7 × 10^{-4} cm^{-1}; g_x, ~2.07, g_y, ~2.07, g_z, ~2.35, and $A_{\parallel}$, ~136.7 × 10^{-4} cm^{-1}), and Fmoc-K/CT-DNA/Cu^{2+} (g_x, ~2.04, g_y, ~2.04, g_z, ~2.34, and $A_{\parallel}$, ~137 × 10^{-4} cm^{-1}) exhibited different spectral characteristics and EPR parameters, suggesting the coordination of Cu^{2+} to both Fmoc-K and CT-DNA. It is worth noting that the spectrum of CT-DNA/Cu^{2+} has a difference between g and A values. The inequality between g_x, g_y and g_z of CT-DNA/Cu^{2+} indicates the asymmetry of the Cu^{2+} coordination sphere, and a larger $A_{\parallel}$ value indicates a weaker coordination environment, which appears to be related to the phosphate groups on the DNA strands. The distinct EPR parameters of the Fmoc-K/CT-DNA/Cu^{2+} complex suggest a synergistically optimized coordination environment.

Subsequently, we investigated the catalytic activities of the self-assembled Cu^{2+} complexes, with 2,4-dichlorophenol (2,4-DCP) and dissolved oxygen as the substrates. In the presence of the catalyst, 2,4-DCP can be oxidized by oxygen to generate semiquinone radicals, which subsequently reacted with 4-aminoantipyrine (4-AP) to form a red-colored adduct with a maximum absorption at 510 nm. Under different Cu^{2+} concentrations, Fmoc-K/CT-DNA/Cu^{2+} exhibited significantly higher activity (estimated as the initial velocity, V_i) than CT-DNA/Cu^{2+} and Fmoc-K/Cu^{2+}, indicating remarkable synergy between

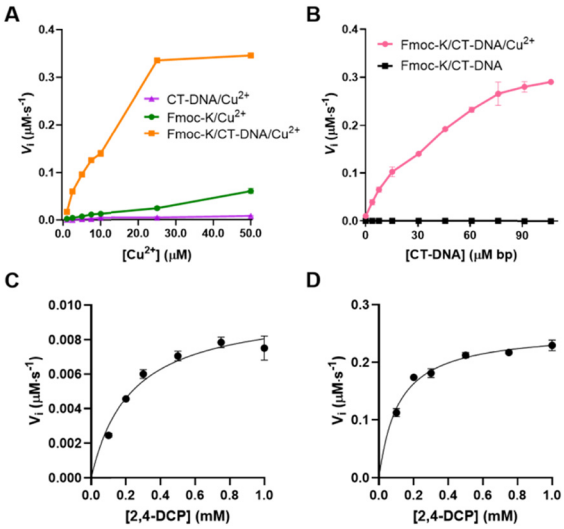

Fig. 3 (A) The initial velocities (V_i) of the indicated Cu^{2+}-containing complexes at various Cu^{2+} concentrations. [Fmoc-K] = 1 mM and [CT-DNA] = 15.2 μM bp. (B) V_i for the Fmoc-K/CT-DNA/Cu^{2+} complex and Fmoc-K at various CT-DNA concentrations. [Cu^{2+}] = 5 μM and [Fmoc-K] = 1 mM. The initial velocities (V_i) of (C) Fmoc-K/Cu^{2+} ([Cu^{2+}] = 5 μM and [Fmoc-K] = 1 mM), (D) CT-DNA/Cu^{2+} ([Cu^{2+}] = 500 μM and [CT-DNA] = 91.2 μM bp) at varying concentrations of 2,4-DCP.

CT-DNA and Fmoc-K in enhancing the reactivity of Cu^{2+} (Fig. 3A). It was also observed that V_i of Fmoc-K/CT-DNA/Cu^{2+} increased rapidly with an increase in the CT-DNA concentration, and reached saturation when the concentration of CT-DNA base-pairs (bp) was up to 91.2 μM bp (Fig. 3B), while the corresponding CT-DNA/Cu^{2+} and Fmoc-K/CT-DNA complexes were inactive. We tested the activities of a variety of transition metals in the presence of the Fmoc-K/CT-DNA hybrid, and found that only the complex containing Cu^{2+} was active (Fig. S7), indicating the specificity of the oxidase mimic to Cu^{2+}. To investigate the enzyme kinetics, we plotted V_i against the substrate (2,4-DCP) concentration in the presence of the different Cu^{2+} complexes. The Michaelis–Menten approach was used to evaluate the turnover rate (k_{cat}) and the catalytic efficiency (k_{cat}/K_M) per Cu^{2+}. The kcat and k_{cat}/K_M values of Fmoc-K/CT-DNA/Cu^{2+} are 0.2876 s^{-1} and 0.1156 s^{-1} mM^{-1}, which were significantly higher than those of CT-DNA/Cu^{2+} (k_{cat}, 0.00051 s^{-1}; k_{cat}/K_M, 0.0045 s^{-1} mM^{-1}) and Fmoc-K/Cu^{2+} (k_{cat}, 0.00198 s^{-1}; k_{cat}/K_M, 0.0086 s^{-1} mM^{-1}) (Fig. 3C, D and Fig. S8 and Table S1). We also observed that Fmoc-K/CT-DNA/Cu^{2+} displayed synergistic activity toward catalyzing oxidation of a range of substrates, including 3,3′,5,5′-tetramethylbenzidine (TMB), and 3,5-di-*tert*-butylcatechol (3,5-DTBC) (Fig. S9). The catalytic efficiency per unit mass of the Fmoc-K/CT-DNA/Cu^{2+} catalyst exhibited 4.66-fold (k_{cat}/K_m = 2.66 μM^{-1} S^{-1} μg^{-1}) higher than that of our previous Fmoc-K/GMP/Cu^{2+} catalyst (k_{cat}/K_m = 0.57 μM^{-1} S^{-1} μg^{-1}),[15] likely because the enhanced affinity between the two ligand-containing components. The remarkable catalytic efficiency of Fmoc-K/CT-DNA/Cu^{2+} assembly confirms a synergistic effect beyond a simple combination of the two components.

It is hypothesized according to our previous work[15] that CT-DNA functions as a co-ligand, with nucleobases (*e.g.*, guanine N7) providing additional nitrogen donors to coordinate with Cu^{2+}, which is primarily chelated by the carboxylate groups of the pre-assembled Fmoc-K scaffold. This hybrid coordination environment likely fine tunes the geometry and electronic structure of the copper center, thereby optimizing it for O_2 binding and activation, analogous to the histidine-coordinated copper sites found in natural laccase. To further validate the proposed mechanism, we performed control experiments. First, to decouple the role of nucleobase coordination from electrostatic effects, we replaced CT-DNA with guanosine triphosphate (GTP) or sodium phosphate (Na_2HPO_3). The catalytic activity was significantly enhanced in the presence of GTP but not Na_2HPO_3 (Fig. S10), demonstrating that nucleobase coordination, rather than interaction with the phosphate backbone, is critical for the activity enhancement. Second, to underscore the necessity of the ordered Fmoc-K assembly, we replaced it with lysine or Boc-lysine (Boc-K). Neither analogue exhibited any notable catalytic activity (Fig. S10), confirming that the π-stacked architecture of Fmoc-K is indispensable for forming the functional catalytic site. These controls collectively confirm that the high activity arises from a unique active site formed only by the synergy between the self-assembled Fmoc-K and the nucleobases of DNA.

The oxidative activity remained unchanged after introducing isopropyl alcohol (IPA, a hydroxyl radical scavenger), 2,2,6,6-tetramethyl-1-piperidinyloxy (TEMPO, a singlet oxygen suppressor), or superoxide dismutase (SOD, a superoxide radical scavenger) into the catalytic system (Fig. S11A). This suggests that Cu^{2+}, rather than reactive oxygen species (ROS), is the key species responsible for oxidizing the reductive substrates, similar to natural laccase. Preliminary evaluation under simulated environmental conditions (*e.g.*, with humic acid[25] and inorganic salts) showed that the catalytic activity remained robust, indicating its potential applicability for remediation in complex water matrices (Fig. S11B).

Thermal stability was evaluated by incubating Fmoc-K/CT-DNA/Cu^{2+} or native laccase (a typical copper-dependent enzyme) at temperatures ranging from 30 to 80 °C. Laccase has an optimal activity at 60 °C but was fully inactivated at 80 °C, which was attributed to the unfolding of the protein and loss of its active site conformation. In contrast, the Fmoc-K/CT-DNA/Cu^{2+} complex showed a 25-fold enhancement of the catalytic activity in the range of 30 to 80 °C (Fig. 4A), demonstrating its remarkable thermal stability. We then compared the storage stabilities of Fmoc-K/CT-DNA/Cu^{2+} and laccase maintained in aqueous solution at room temperature. Fmoc-K/CT-DNA/Cu^{2+} did not show inactivation over as long as 32 days, while laccase was almost inactivated, demonstrating the superior storage stability of the synthetic catalyst (Fig. 4B). The pH-dependent activity of the Fmoc-K/CT-DNA/Cu^{2+} complex was also evaluated (Fig. S11C), and the catalytic activity increased with an increase in pH from 4.2 to 7.8.

Pharmaceutical pollution has been demonstrated to have detrimental effects on ecosystems and human health. Double stranded DNA (*e.g.* CT-DNA) has been reported to interact with

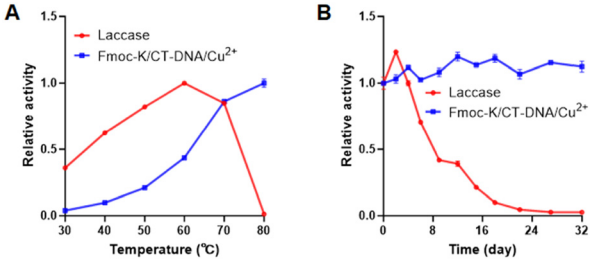

Fig. 4 (A) Temperature-dependent catalytic rates (relative activity) of laccase and Fmoc-K/CT-DNA/Cu^{2+}. [laccase] = 1 μM, [Cu^{2+}] = 0.5 μM, [Fmoc-K] = 1 mM, and [CT-DNA] = 15.2 μM bp. (B) Storage stability of laccase and Fmoc-K/CT-DNA/Cu^{2+} at room temperature. [laccase] =1 μM, [Cu^{2+}] = 5 μM, [Fmoc-K] = 1 mM, [CT-DNA] = 15.2 μM bp. [2,4-DCP] = 1 mM, and [4-AP] = 1 mM.

antibiotics through a combination of noncovalent interactions, intercalation and groove binding,[26,27] which can facilitate the access of the antibiotics to the copper center. In this work, we explored the potential of the Fmoc-K/CT-DNA/Cu^{2+} complex in catalyzing degradation of doxorubicin (DOX) and tetracycline (TC), which have been widely used as a broad-spectrum antineoplastic drug to treat cancers. As illustrated in (Fig. S12A), the UV-vis absorption spectrum demonstrates a decrease in the peak at 500 nm, indicating the interaction between DOX and the CT-DNA.[28,29] Upon the addition of Cu^{2+}, a red-shift occurs, accompanied by the emergence of a new peak at 585 nm, indicative of the formation of the DOX/CT-DNA/Cu^{2+} complex. Furthermore, upon the introduction of Fmoc-K, only a slight alteration in the spectrum is observed, suggesting that the structure of the DOX/CT-DNA-DOX/Cu^{2+} complex was retained. The formation of the DOX/CT-DNA-TC/Cu^{2+} complex was demonstrated in a similar manner (Fig. S12B). Our findings revealed a significant increase in the degradation efficiency of DOX and TC in the presence of the Fmoc-K/CT-DNA/Cu^{2+} complex, surpassing that observed in the Fmoc-K/Cu^{2+} and CT-DNA/Cu^{2+} systems (Fig. 5A and B). Elevation of temperatures further improved the degradation efficiency (Fig. S13 and S14). These results indicate that the interactions of DOX or TC with CT-DNA play a critical role in promoting the degradation process.

Then, we analyzed the degradation products by liquid chromatography–mass spectrometry (LC-MS) (Fig. S15 and S16). For DOX degradation, the DP1 product was the amino ribose moiety cleaved *via* hydrolysis, and DP2, DP3, and DP4 products were generated through ring-opening reactions of the anthraquinone ring (Fig. 5C). For TC degradation, the TP1 product was formed *via* demethylation, and TP2, TP3, TP4, and TP5 products were produced through ring-opening pathways (Fig. 5D). To evaluate the toxicity of the degradation products, we employed the quantitative structure–activity relationship (QSAR) method using the Toxicity Estimation Software Tool (T.E.S.T) to predict the 96-h LC_{50} (lethal concentration for 50% of fathead minnows). The degradation products of DOX (DP1–DP4) and those of TC (TP4–TP5) exhibited higher LC_{50} values compared with DOX and TC, respectively (Fig. S17). Furthermore, the fragmentation of key molecular structures (*e.g.*, the quinone moiety), as identified by LC-MS, suggests a loss of the antibiotic pharmacophore.[30]

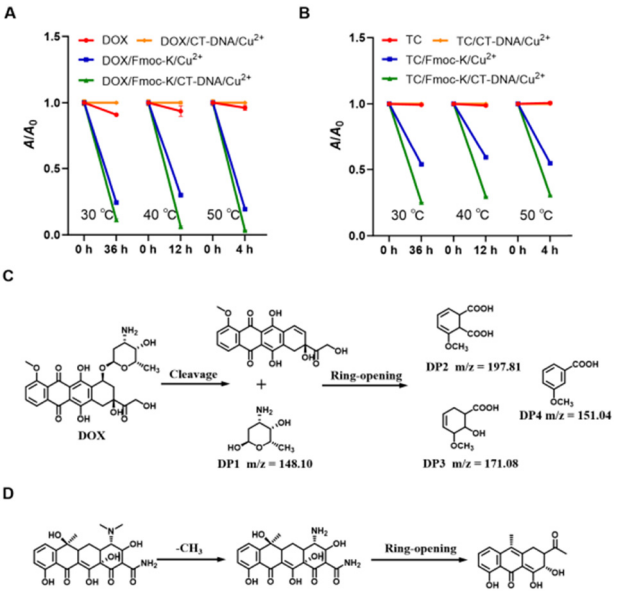

Fig. 5 Ratio of the concentration of (A) DOX or (B) TC to their initial concentration (A/A_0) after a certain reaction time. [Cu^{2+}] = 5 μM, [Fmoc-K] = 1 mM, [CT-DNA] = 45.6 μM bp, [DOX] = 24 μM, and [TC] = 24 μM. (C) Proposed degradation pathway for DOX. (D) Proposed degradation pathway for TC.

This, coupled with the reduced toxicity, indicates that the degradation products are unlikely to retain significant biological activity or pose a substantial risk for inducing antibiotic resistance. These findings suggest that the catalytic transformation of DOX and TC by the Fmoc-K/CT-DNA/Cu^{2+} complex effectively reduces the toxicity of both antibiotics.

Conclusions

In summary, our study presents the self-assembly of calf thymus DNA (CT-DNA) with Fmoc-lysine (Fmoc-K) and Cu^{2+}, resulting in the formation of a supramolecular enzyme mimic with polyphenol oxidase activity. Notably, the interaction between CT-DNA and Fmoc-K plays a critical role in the improvement of catalytic activity. Unlike native laccase, the catalyst exhibited temperature-dependent activity, where catalytic efficiency increased with increasing reaction temperatures, and maintained exceptional stability when stored in buffer at room temperature. Additionally, the interaction of CT-DNA with doxorubicin and tetracycline facilitated the catalytic degradation of these antibiotics. This work highlights the unique advantages of DNA in constructing multi-component supramolecular catalysts, and provides a novel strategy for developing functional supramolecular catalysts with tailored applications.

Experimental

Materials

Fmoc-lysine-OH·HCl (Fmoc-K), copper sulfate pentahydrate ($CuSO_4·5H_2O$), cobalt chloride hexahydrate ($CoCl_2·6H_2O$), zinc acetate ($C_4H_6O_4Zn$), aluminum chloride ($AlCl_3$), strontium chloride hexahydrate ($SrCl_2·6H_2O$), cadmium chloride ($CdCl_2$), manganese chloride ($MnCl_2$), 2-4-dichlorophenol (2,4-DCP), 4-aminoantipyrine (4-AP), 3,3′,5,5′-tetramethyl-benzidine (TMB), 3,5-di-*tert*-butylcatechol (3,5-DTBC), and dimethyl sulfoxide (DMSO) were purchased from Aladdin (China). Laccases and superoxide dismutase (SOD) were purchased from Yuanye (China). Scandium chloride hexahydrate ($ScCl_3·6H_2O$), thioflavin T (ThT), doxorubicin (DOX) and tetracycline (TC) were purchased from Bidepharm. Nickel chloride hexahydrate ($NiCl_2·6H_2O$), anhydrous magnesium sulfate ($MgSO_4$) and 2,2,6,6-tetramethylpiperidine (TEMP) were purchased from Macklin. Vanadium chloride (VCl_3) and isopropyl alcohol were purchased from Energy Chemical.

Calf thymus DNA (CT-DNA, an average molecular weight of seven million) was purchased from Solarbio. Water was deionized using a Milli-Q system (≥18.25 MΩ cm).

Instruments

TEM characterization was conducted using a Hitachi 7800 microscope in bright-field mode at 80 kV. Fluorescence emission spectra were recorded using a G9800A fluorescence spectrophotometer with a temperature-control accessory (Agilent Technologies). CD spectra were recorded with a J-815 spectropolarimeter (Jasco) under the following conditions: optical path, 0.5 mm; bandwidth, 10 nm; scan speed, 50 nm min^{-1}. UV-vis absorption spectra were recorded using a UV-2600 spectrometer equipped with a temperature-control accessory (Shimadzu). Mass spectroscopy (MS) was conducted using an Agilent G6500 series liquid chromatograph with electrospray ionization (ESI).

Sample preparation for TEM

Fmoc-K, CT-DNA and Cu^{2+} were dissolved in water and mixed at room temperature. A 6 μL aliquot of the self-assembled sample solution was deposited onto a hydroxylated copper sheet and allowed to stand overnight for solvent evaporation.

Activity assay

The amino acid amphiphile (Fmoc-K) was dissolved in ultrapure water to prepare a 100 mM stock solution. After being stored for one month, the solution was lyophilized into a powder and later reconstituted for use. Calf thymus DNA (CT-DNA) was dissolved in ultrapure water to prepare a 1 mg mL^{-1} stock solution. Desired concentrations of the amino acid amphiphile, CT-DNA, and copper ions were then added to a 20 mM acetate buffer. The initial catalytic velocity (V_i) and apparent kinetic parameters were determined by monitoring the time-dependent absorbance changes at 510 nm using 2,4-DCP/4-AP as the reductive substrate.

For the DOX and TC degradation experiments, the degradation efficiency was evaluated by measuring the decrease in absorbance at 500 nm and 360 nm, respectively.

Author contributions

Z. G. W. conceived, designed, and supervised the experiments. X. Z. and M. Y. designed and performed the experiments.

Z. G. W., M. Y. and X. Z. collected and analyzed the data. S. X. performed the simulations. Z. G. W., M. Y. and X. Z. wrote the manuscript. All authors have given approval to the final version of the manuscript.

Conflicts of interest

There are no conflicts to declare.

Data availability

The data that support the findings of this study are available from the corresponding author upon reasonable request.

Supplementary information (SI) is available. See DOI: https://doi.org/10.1039/d5nh00492f.

Acknowledgements

The authors are grateful for the support from Beijing Natural Science Foundation (2232017), the National Natural Science Foundation of China (52173194), and the Fundamental Research Funds for the Central Universities (buctrc201902). The structural simulation is supported by the Hefei Advanced Computing Center and High-Performance Computing Platform of BUCT.

References

1 I. T. Carvalho and L. Santos, Antibiotics in the aquatic environments: A review of the European scenario, *Environ. Int.*, 2016, **94**, 736–757.
2 S. Zheng, Y. Wang, C. Chen, X. Zhou, Y. Liu, J. Yang, Q. Geng, G. Chen, Y. Ding and F. Yang, Current Progress in Natural Degradation and Enhanced Removal Techniques of Antibiotics in the Environment: A Review, *Int. J. Environ. Res. Public Health*, 2022, **19**(17), 10919.
3 T. Rosado, P. Bernardo, K. Koci, A. V. Coelho, M. P. Robalo and L. O. Martins, Methyl syringate: An efficient phenolic mediator for bacterial and fungal laccases, *Bioresour. Technol.*, 2012, **124**, 371–378.
4 J. Su, J. Fu, Q. Wang, C. Silva and A. Cavaco-Paulo, Laccase: a green catalyst for the biosynthesis of poly-phenols, *Crit. Rev. Biotechnol.*, 2017, **38**(2), 294–307.
5 Y. Xia, L. Xia and X. Lin, Laccase-Based Self-Amplifying Catalytic System Enables Efficient Antibiotic Degradation for Sustainable Environmental Remediation, *Adv. Sci.*, 2023, **10**(21), 2300210.
6 Y. Wu, Y. Teng, Z. Li, X. Liao and Y. Luo, Potential role of polycyclic aromatic hydrocarbons (PAHs) oxidation by fungal laccase in the remediation of an aged contaminated soil, *Soil Biol. Biochem.*, 2008, **40**(3), 789–796.
7 S. Mukherjee, B. Basak, B. Bhunia, A. Dey and B. Mondal, Potential use of polyphenol oxidases (PPO) in the bioremediation of phenolic contaminants containing industrial wastewater, *Rev. Environ. Sci. Biotechnol.*, 2012, **12**(1), 61–73.
8 L. A. Solomon, J. B. Kronenberg and H. C. Fry, Control of Heme Coordination and Catalytic Activity by Conformational Changes in Peptide–Amphiphile Assemblies, *JACS Au*, 2017, **139**(25), 8497–8507.
9 T. Pan, Y. Wang, X. Xue and C. Zhang, Rational design of allosteric switchable catalysts, *Exploration*, 2022, **2**(2), 20210095.
10 Y. Yuan, L. Chen, L. Kong, L. Qiu, Z. Fu, M. Sun, Y. Liu, M. Cheng, S. Ma, X. Wang, C. Zhao, J. Jiang, X. Zhang, L. Wang and L. Gao, Histidine modulates amyloid-like assembly of peptide nanomaterials and confers enzyme-like activity, *Nat. Commun.*, 2023, **14**(1), 5808.
11 H. Liang, F. Lin, Z. Zhang, B. Liu, S. Jiang, Q. Yuan and J. Liu, Multicopper Laccase Mimicking Nanozymes with Nucleotides as Ligands, *ACS Appl. Mater. Interfaces*, 2017, **9**(2), 1352–1360.
12 J. Wang, R. Huang, W. Qi, R. Su, B. P. Binks and Z. He, Construction of a bioinspired laccase-mimicking nanozyme for the degradation and detection of phenolic pollutants, *Appl. Catal., B*, 2019, **254**, 452–462.
13 J. Wang, R. Huang, W. Qi, R. Su and Z. He, Construction of biomimetic nanozyme with high laccase- and catecholase-like activity for oxidation and detection of phenolic compounds, *J. Hazard. Mater.*, 2022, **429**, 128404.
14 G. Zhang, Y. Liang, Y. Wang, Q. Li, W. Qi, W. Zhang, R. Su and Z. He, Chirality-Dependent Copper–Diphenylalanine Assemblies with Tough Layered Structure and Enhanced Catalytic Performance, *ACS Nano*, 2022, **16**(4), 6866–6877.
15 S. Xu, H. Wu, S. Liu, P. Du, H. Wang, H. Yang, W. Xu, S. Chen, L. Song, J. Li, X. Shi and Z.-G. Wang, A supramolecular metalloenzyme possessing robust oxidase-mimetic catalytic function, *Nat. Commun.*, 2023, **14**(1), 4040.
16 X. Zhang, X. Liu, D. L. Phillips and C. Zhao, Mechanistic Insights Into the Factors That Influence the DNA Nuclease Activity of Mononuclear Facial Copper Complexes Containing Hetero-Substituted Cyclens, *ACS Catal.*, 2015, **6**(1), 248–257.
17 L.-M. Cao, C.-G. Hu, H.-H. Li, H.-B. Huang, L.-W. Ding, J. Zhang, J.-X. Wu, Z.-Y. Du, C.-T. He and X.-M. Chen, Molecule-Enhanced Electrocatalysis of Sustainable Oxygen Evolution Using Organoselenium Functionalized Metal–Organic Nanosheets, *JACS Au*, 2022, **145**(2), 1144–1154.
18 X. Hou, H. Wang, L. Jia, M. Li, W. Yu and Z. Bian, Nitrogen-doped carbon bilayer flow-through electrocatalytic membrane based on transition metal single atoms: Simultaneous generation and activation of H_2O_2 for ibuprofen degradation, *Chem. Eng. J.*, 2025, **513**, 162950.
19 A. M. Smith, R. J. Williams, C. Tang, P. Coppo, R. F. Collins, M. L. Turner, A. Saiani and R. V. Ulijn, Fmoc-Diphenylalanine Self Assembles to a Hydrogel *via* a Novel Architecture Based on π–π Interlocked β-Sheets, *Adv. Mater.*, 2007, **20**(1), 37–41.
20 C. Tang, R. V. Ulijn and A. Saiani, Self-assembly and gelation properties of glycine/leucine Fmoc-dipeptides, *Eur. Phys. J. E: Soft Matter Biol. Phys.*, 2013, **36**(10), 111.
21 K. Tao, E. Yoskovitz, L. Adler-Abramovich and E. Gazit, Optical property modulation of Fmoc group by pH-dependent self-assembly, *RSC Adv.*, 2015, **5**(90), 73914–73918.

22 V. Basavalingappa, S. Bera, B. Xue, I. Azuri, Y. Tang, K. Tao, L. J. W. Shimon, M. R. Sawaya, S. Kolusheva, D. S. Eisenberg, L. Kronik, Y. Cao, G. Wei and E. Gazit, Mechanically rigid supramolecular assemblies formed from an Fmoc-guanine conjugated peptide nucleic acid, *Nat. Commun.*, 2019, **10**(1), 5256.
23 F. Yeasmin Khusbu, X. Zhou, H. Chen, C. Ma and K. Wang, Thioflavin T as a fluorescence probe for biosensing applications, *TrAC, Trends Anal. Chem.*, 2018, **109**, 1–18.
24 P. Hanczyc, P. Rajchel-Mieldzioć, B. Feng and P. Fita, Identification of Thioflavin T Binding Modes to DNA: A Structure-Specific Molecular Probe for Lasing Applications, *J. Phys. Chem. Lett.*, 2021, **12**(22), 5436–5442.
25 C. Plaza, G. Brunetti, N. Senesi and A. Polo, Molecular and Quantitative Analysis of Metal Ion Binding to Humic Acids from Sewage Sludge and Sludge-Amended Soils by Fluorescence Spectroscopy, *Environ. Sci. Technol.*, 2006, **40**, 917–923.
26 A. A. Almaqwashi, T. Paramanathan, I. Rouzina and M. C. Williams, Mechanisms of small molecule–DNA interactions probed by single-molecule force spectroscopy, *Nucleic Acids Res.*, 2016, **44**(9), 3971–3988.
27 K. Lozano Untiveros, E. G. da Silva, F. C. de Abreu, E. F. da Silva-Júnior, J. X. de Araújo-Junior, T. Mendoça de Aquino, S. M. Armas, R. O. de Moura, F. J. B. Mendonça-Junior, V. L. Serafim and K. Chumbimuni-Torres, An electrochemical biosensor based on Hairpin-DNA modified gold electrode for detection of DNA damage by a hybrid cancer drug intercalation, *Biosens. Bioelectron.*, 2019, **133**, 160–168.
28 H. Ijäs, B. Shen, A. Heuer-Jungemann, A. Keller, M. A. Kostiainen, T. Liedl, J. A. Ihalainen and V. Linko, Unraveling the interaction between doxorubicin and DNA origami nanostructures for customizable chemotherapeutic drug release, *Nucleic Acids Res.*, 2021, **49**(6), 3048–3062.
29 E. V. Dukhopelnykov, Y. N. Blyzniuk, A. A. Skuratovska, E. G. Bereznyak and N. A. Gladkovskaya, Interaction of doxorubicin delivered by superparamagnetic iron oxide nanoparticles with DNA, *Colloids Surf., B*, 2022, **219**, 112815.
30 M. de Almeida Ultramari, A. Rivellis Julio, L. Souza Passos, A. Ossanes de Souza, N. Pereira da Silva, P. N. Nunes de Freitas and E. Pinto, Doxorubicin Stability-indicating Method and its Main Degradation Products In vitro Toxicity, *AAPS J.*, 2025, **27**(5), 117.